CCS Chemistry

RESEARCH ARTICLE

Received: Oct. 10, 2023 | Accepted: Jan. 2, 2024 | Published: Feb. 1, 2024

Recyclable Perovskite Solar Cells with Lead Sulfate Contact

Guo-Bin Xiao[1†], Xijiao Mu[1†], Luyao Wang[2†], Zhen-Yang Suo[1†], Artem Musiienko[3], Guixiang Li[3], Zeying Guo[1], Yiying Wu[4], Antonio Abate[3] & Jing Cao[1*]

[1]State Key Laboratory of Applied Organic Chemistry, Key Laboratory of Nonferrous Metal Chemistry and Resources Utilization of Gansu Province, College of Chemistry and Chemical Engineering, Lanzhou University, Lanzhou 730000, [2]State School of Materials Science and Engineering, Shanghai Jiao Tong University, Shanghai 200240, [3]Department Novel Materials and Interfaces for Photovoltaic Solar Cells, Helmholtz-Zentrum Berlin für Materialien und Energie, 12489 Berlin, [4]Department of Chemistry and Biochemistry, The Ohio State University, Columbus, Ohio 43210

**Corresponding author: caoj@lzu.edu.cn; †G.-B. Xiao, X. J. Mu, L. Y. Wang, and Z. Y. Suo contributed equally to this work.*

Cite this: *CCS Chem.* **2024**, 6, 2254–2263
DOI: 10.31635/ccschem.024.202303502

Previous cost analysis of perovskite solar cells (PSCs) has revealed that the transparent conductive oxide (TCO) substrates account for most of the material cost, emphasizing the need to recover TCO in PSC recycling. However, the conventional use of compact and ultrathin electron transport materials (ETMs) such as TiO_2 and SnO_2, poses a challenge to their removal from the substrate, hindering effective PSC recycling. Here, $PbSO_4$ nanoparticles with (011) surface were used as ETM to fabricate PSCs. The yielded metallicity on the $PbSO_4$ nanoparticle surface promoted extracted electron transport across the nanoparticle surface. A certified efficiency as high as 17.9% for the submodule (204.9 cm^2) with $PbSO_4$ was realized successfully, and the best efficiency on a small area (0.1 cm^2) reached 24.1%. The $PbSO_4$ layer was removed effortlessly from the substrate by simple aminoethanol washing to recover the TCO, the most expensive component of PSCs. This work provides a novel strategy to prepare soluble insulator-based ETMs by constructing metallic surfaces of nanoparticles; thus, fabricating efficient and recyclable PSCs.

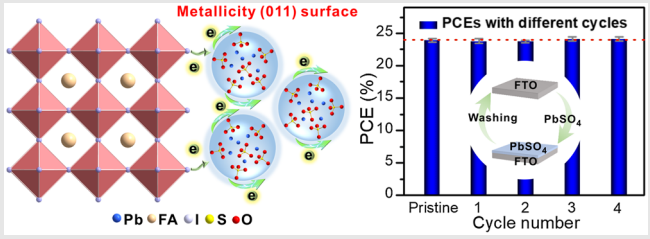

Keywords: **wide-bandgap, surface metallicity, electron transport material, perovskite solar cells, recyclability**

Introduction

With the increase in global energy demand, clean energy development has been stimulated to a new level. In recent years, all types of solar cells have been rapidly developed, including silicon (Si), dye-sensitized solar cells (DSSCs), organic photovoltaic (OPV), cadmium telluride (CdTe), copper indium gallium selenide (CIGS), and organic–inorganic halide perovskite solar cells (PSCs). Among all these technologies, PSCs have come into research focus due to their high absorption coefficient, long carrier diffusion length, tunable bandgaps, and ease of fabrication technology.[1-6] The power conversion efficiency (PCE) of PSCs with an *n–i–p* architecture has reached up to 26.0%.[7-10] In the configuration of PSCs, the electron transport materials (ETMs) can effectively promote interfacial electron extraction and transport, block free holes, and suppress charge recombination.[11-16] Thus, preparing ETMs is crucial for fabricating efficient and stable PSCs.

Tremendous efforts have been devoted to the optimization and designing of efficient ETMs for PSCs. To date,

TiO_2 and SnO_2 are typically used as the ETMs to fabricate highly efficient PSCs.[17–22] For instance, the SnO_2 layer with ideal coverage, composition, and thickness could be prepared by chemical bath deposition (CBD) to improve charge carrier management, thereby realizing the certified PCE of 25.2%.[23] The compact-TiO_2 modified with a thin layer of polyacrylic acid-stabilized tin(IV) oxide quantum dots (paa-QD-SnO_2), used as electron-selective contact-enabled PSCs, could enhance the light capture and suppress nonradiative recombination, enabling their PCE up to 25.7% (certified 25.4%).[24] The chlorine-bound SnO_2 electron transport layer enhanced charge extraction and transport from the perovskite layer. A certified power electronic converter (PEC) of 25.5% was achieved.[25] However, the conventional use of ETMs is difficult to remove from the substrates, hindering the effective recovery of transparent conductive oxide (TCO) substrates, which accounts for 58–73% of the material cost in PSCs.[26,27] Therefore, the design and preparation of new type soluble inorganic ETMs is critical for recycling TCO substrates in PSCs.

$PbSO_4$ is used as a perovskite surface passivation layer and has been used to improve the efficiency and stability of PSC.[28] However, the wide bandgap of $PbSO_4$ makes it challenging to reach an effective electron transport, impeding the applications in PSCs as ETMs. Constructing surface metallicity has been demonstrated as a useful way to boost the charge transport ability in insulating nanomaterials.[29–31] Here, $PbSO_4$ nanoparticles with (011) surface were coated on a conductive substrate to fabricate PSCs. The formed metallicity on the (011) surface of the $PbSO_4$ nanoparticle boosted the transport of extracted electrons across the nanoparticle surface. The resultant PSCs with $PbSO_4$ achieved over 24% performance and remarkable stability over 3000 h under light stress. A certified efficiency as high as 17.9% for the submodule (204.9 cm^2) with $PbSO_4$ was successfully realized. More strikingly, the $PbSO_4$ film on fluorine-doped tin oxide (FTO) could be separated entirely by aminoethanol washing to recover the expensive FTO substrate. Thus, efficient and recyclable PSCs were fabricated successfully.

Experimental Methods

All reagents and materials are directly used as purchased from chemical companies without any further purification. Detailed experiments involving solar cell fabrication, computational parameters, and device characterization are provided in the Supporting Information.

Solar cell fabrication

FTO glass with an electrode pattern was used as a conductive substrate. $PbSO_4$ solution was spin-coated on the FTO substrate at 5,000 rpm for 25 s, annealed at 100 °C 15 min, 200 °C for 30 min and mesoporous TiO_2 was spin-coated at 5000 rpm for 25 s, annealed at 500 °C for 30 min, both used as alternate negative charge extraction layer or electron transport materials. The perovskite precursor solution was spin-coated in a nitrogen-filled glove box, and coated 2,2′,7,7′-tetrakis-(*N*,*N*-di-*p*-methoxyphenylamine)-9,9′-spiro-bifluorene (Spiro-OMeTAD) and phthalocyanine were used as the hole transport layer, which sandwiched the perovskite layer and the negative charge extraction layer. Finally, a gold electrode (80 nm) was deposited by thermal evaporation.

Computational methods

The first-principles calculation steps were completed through structural optimization, static self-consistent field, and density of state calculation with spin-orbital coupling. All calculation steps were completed using Quantum-Espresso (https://www.quantum-espresso.org/), combined with the generalized gradient approximation in density functional theory (DFT). The Monte Carlo method (https://sourceforge.net/) was used to simulate the accumulation of nanoparticles of varying sizes within a defined space and to determine the path of the electric current.

Device characterizations

The current density–voltage (*J*–*V*) tests of PSCs were performed on a solar simulator equipped with an LSH-7320 ABA LED solar simulator (Newport, California, USA) and Keithley 2400 source meter (Keithley, Ohio, USA). The light intensity was calibrated to 100 mW cm^{-2} with the certified Oriel 91150V silicon solar cell (Newport). Scanning electron microscopy (SEM) images were measured on an Apreo S 2 microscope (Thermo Fisher Scientific, Shanghai, China). Atomic force microscopy (AFM) and kelvin probe force microscopy (KPFM) tests were measured on Dimension Icon-Raman AFM (Bruker, Saarbrücken, Germany). Mott–Schottky, space charge limitation current and electrical impedance spectroscopy tests were performed using the CHI660E electrochemical workstation (ChenHua, XXX, XXX). Ultraviolet–visible (UV–vis) absorption spectra were recorded by Cary-5000 UV–vis spectrophotometer (Agilent, XXX, XXX). Photoluminescence (PL) spectra were measured on FL-3 (Horiba, XXX, XXX).

Results and Discussion

Recycling the compact TiO_2 and SnO_2-coated substrates

Compact TiO_2 (c-TiO_2) and SnO_2 as commonly used ETMs are challenging to remove from the FTO substrates, which hinders the recovery of FTO. To verify this

DOI: 10.31635/ccschem.024.202303502
Citation: *CCS Chem.* **2024**, 6, 2254–2263
Link to VoR: https://doi.org/10.31635/ccschem.024.202303502

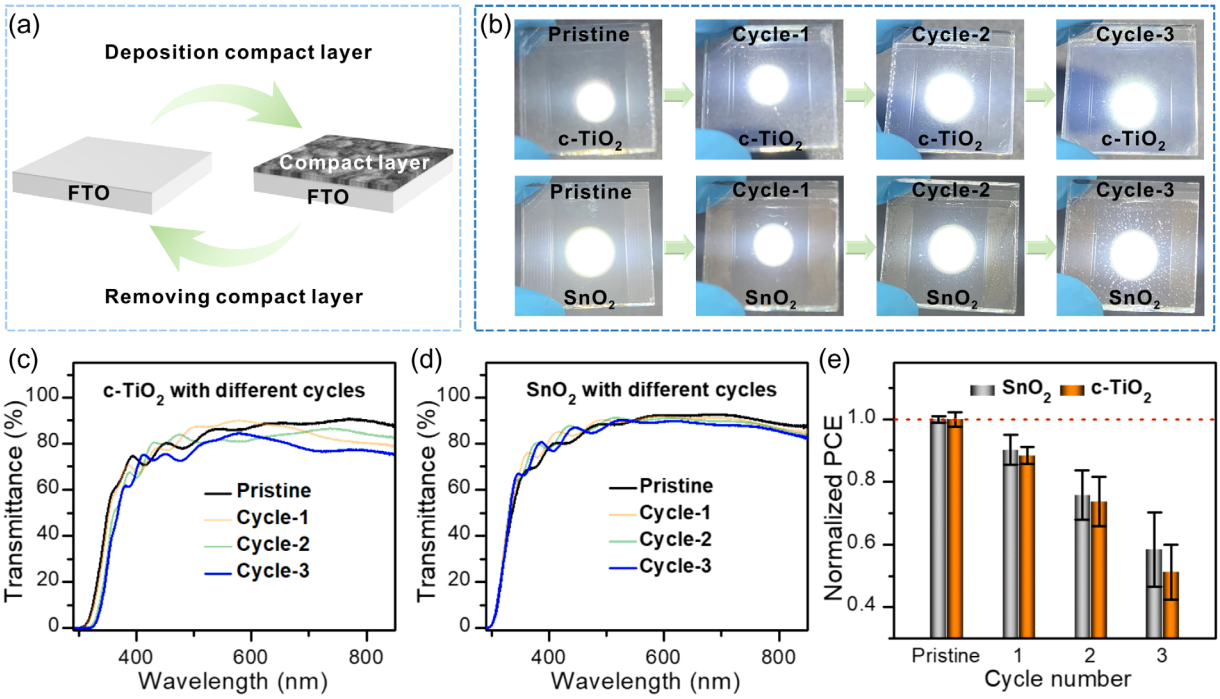

Figure 1 | *(a) Roadmap for recycling of conductive substrates. (b) Photos of recovered substrates at different cycles. Transmission spectra of substrates with c-TiO_2 (c) and SnO_2 (d) at different cycles. (e) Efficiencies of PSCs with SnO_2 and c-TiO_2 at different cycles.*

issue, the c-TiO_2 and SnO_2-coated substrates were prepared and then washed with *N*,*N*-dimethylformamide (DMF), ethanol, and distilled water, respectively (Figure 1a). After washing several times, the recycled substrates exhibited much rougher surface morphologies (Figure 1b). A decrease in transmittance was also observed (Figure 1c,d). PSCs with FTO/c-TiO_2 or SnO_2/perovskite/Spiro-OMeTAD/Au configuration were fabricated with recycled substrates. As shown in Figure 1e, the efficiency of devices with c-TiO_2 and SnO_2 lost >40% of their initial efficiency after three cycles. These results demonstrated that the convenient and feasible methods could not efficiently recover the substrates with c-TiO_2 and SnO_2 ETMs.

Properties analyses of $PbSO_4$ film

This work developed a fully recyclable ETM, the $PbSO_4$ powder was dissolved into an ethanolamine solution and directly deposited on the FTO substrate to fabricate PSCs (Figure 2a). It is worth highlighting that the material cost of $PbSO_4$ was only ~4% of the cost of commonly used SnO_2/TiO_2 ETMs in PSCs (Figure 2b).[32] X-ray diffraction (XRD) pattern of the deposited film agreed with the simulated values from single crystal data of $PbSO_4$ (Supporting Information Figure S1), proving the successful deposition of $PbSO_4$ on the FTO substrate. The high-angle annular dark field aberration-corrected scanning transmission electron microscopy (HAADF-Cs-STEM) confirmed the prepared $PbSO_4$ nanoparticle with exposed (011) facets (Figure 2c). Theoretical calculations of $PbSO_4$ surface energy revealed that the (011) surface exhibited the most negative surface energy (Supporting Information Table S1), indicating that it was readily exposed to the (011) surface during the formation process. Scanning electron microscopy (SEM) and atomic force microscopy (AFM) images indicated that the $PbSO_4$ nanoparticles were uniformly distributed on the FTO surface to reduce the surface roughness (Supporting Information Figures S2 and S3). AFM images suggested the thickness of the $PbSO_4$ thin layer was ~20 nm (Figure 2d,e). The FTO substrate coated with $PbSO_4$ revealed an enhanced transmittance than the TiO_2-coated FTO film, suggesting that the $PbSO_4$ film is optically suitable as ETM (Supporting Information Figure S4).

The energy band structure and work function (W_F) of $PbSO_4$ film on FTO substrate were investigated by ultraviolet photoelectron spectroscopy (UPS) (Figure 2f,g and Supporting Information Figure S5). The calculated W_F for the pristine FTO and $PbSO_4$-modified FTO were −4.25 and −4.37 eV, respectively. The conduction band minimum (E_{CBM}) of FTO and $PbSO_4$-modified FTO evaluated were −4.26 and −3.38 eV, respectively. DFT calculation results suggested that the work function of the $PbSO_4$ (011) surface was −3.13 eV (Supporting Information Figure S6), consistent with the value

DOI: 10.31635/ccschem.024.202303502
Citation: *CCS Chem.* **2024**, 6, 2254–2263
Link to VoR: https://doi.org/10.31635/ccschem.024.202303502

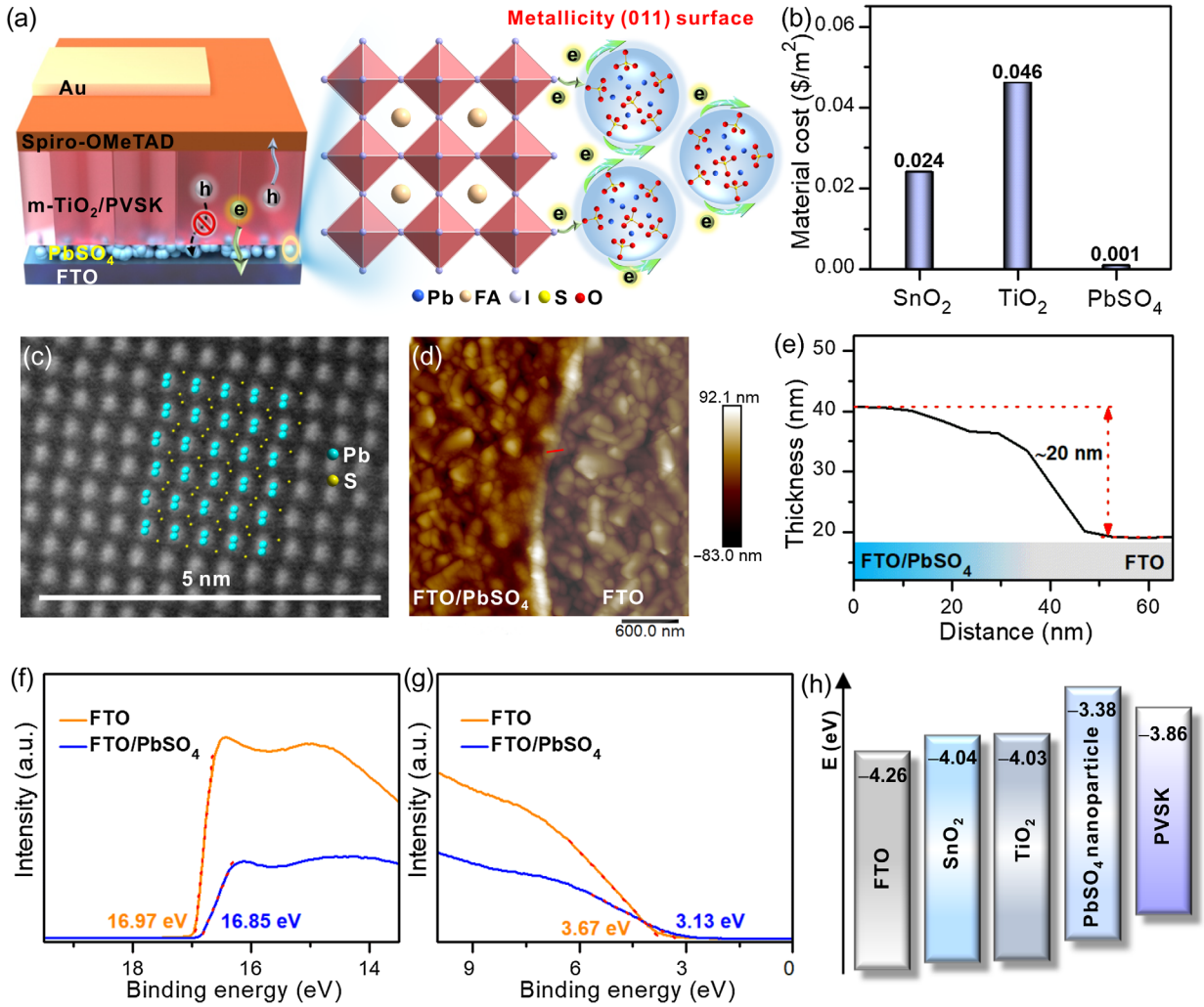

Figure 2 | *(a) Scheme of electron transport from perovskite (PVSK) to substrate in PSC. (b) Costs of SnO_2, TiO_2, and $PbSO_4$ in PSCs. (c) HAADF-Cs-STEM image of $PbSO_4$ with (011) surface. (d) AFM image of FTO/$PbSO_4$ substrate. (e) Thickness of $PbSO_4$ thin layer. Electron cut-off region (f) and valence band region (g) of UPS spectra of FTO and FTO/$PbSO_4$. (h) Energy band alignment of FTO, SnO_2, TiO_2, $PbSO_4$ nanoparticle, and PVSK.*

obtained from UPS characterization results. Thus, the $PbSO_4$-modified FTO had a higher conduction band energy level than perovskite, as shown in Figure 2h, which is beneficial for suppressing interfacial charge recombination.

Analyses of the electron transport process

Detailed experimental characterizations were conducted to assess the positive effect of $PbSO_4$ on interfacial electron transport. First, the characteristics of perovskite films based on different ETMs were studied. The XRD patterns (Supporting Information Figure S7) and UV–vis spectra (Supporting Information Figure S8) of the perovskite films coated on other substrates indicated that the $PbSO_4$ layer did not affect the component and optical properties of the perovskite film. As shown in Figure 3a–d, the perovskite films with TiO_2 and $PbSO_4$ revealed similar uniform and dense morphologies. The flatter morphology for $PbSO_4$-based perovskite film with a root mean square (RMS) of 10.5 nm was observed more than that of the TiO_2 (RMS: 11.9 nm) (Supporting Information Figure S9). Thus, the $PbSO_4$ layer could be used to prepare high-quality perovskite films.

The electron transport property of $PbSO_4$ with (011) surface was further assessed. Surface spin–orbit coupling (SOC) electronic structure revealed that the electron transport in $PbSO_4$ nanoparticle was dependent on the O-exposed (011) surface state (Figure 3e and Supporting Information Figure S10). Moreover, the conduction band and valence band touched each other, resulting in a metallic band structure. The SOC of O and Pb led to the surface energy band crossing over the fermi level, degenerating the two energy bands to form a new metal

DOI: 10.31635/ccschem.024.202303502
Citation: *CCS Chem.* **2024**, 6, 2254–2263
Link to VoR: https://doi.org/10.31635/ccschem.024.202303502

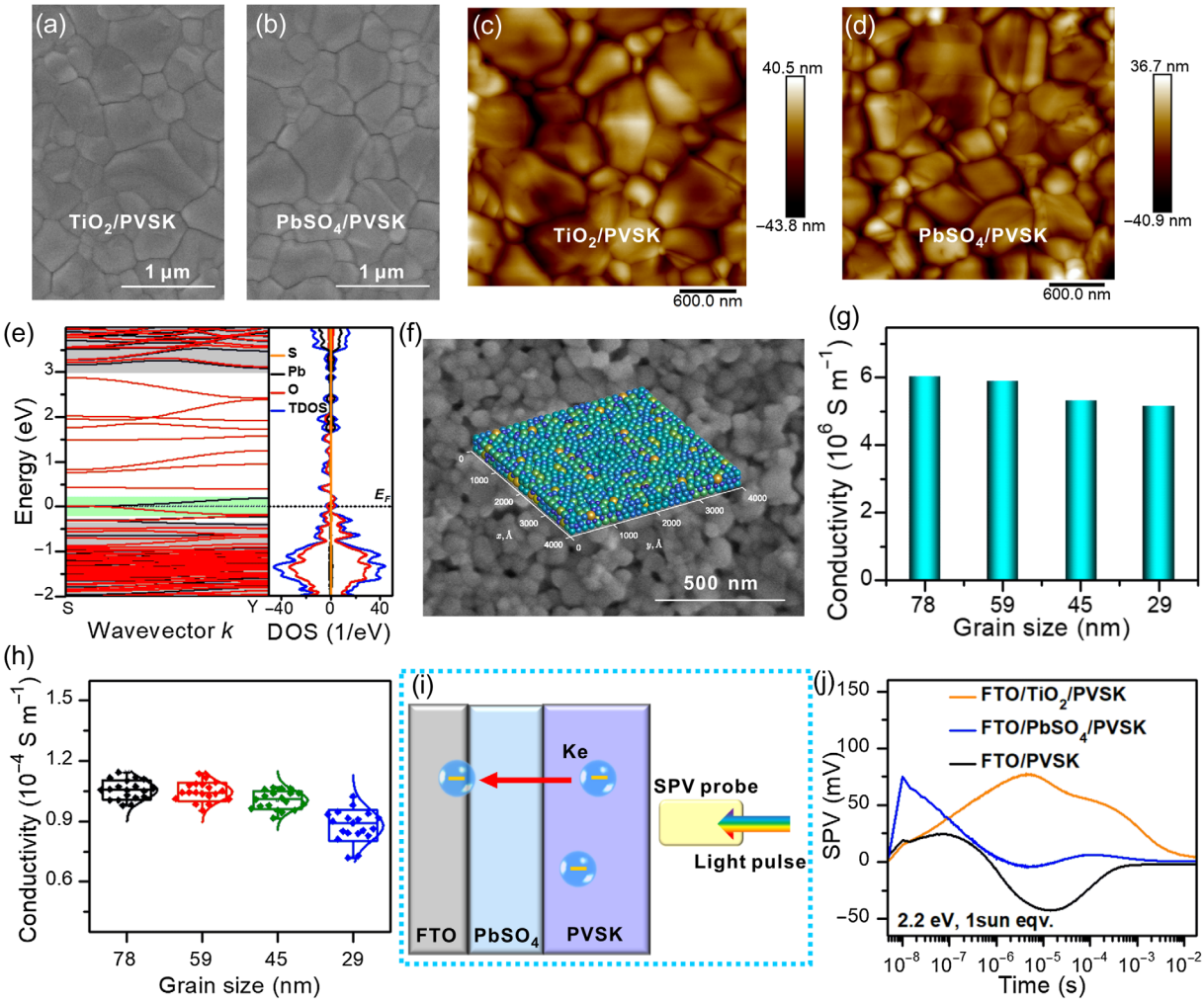

Figure 3 | *SEM images of perovskite films with TiO_2 (a) and $PbSO_4$ (b). AFM images of perovskite films with TiO_2 (c) and $PbSO_4$ (d). (e) Surface SOC electronic structure of $PbSO_4$ (011) surface. (f) SEM images of $PbSO_4$ nanoparticles (the inset is Monte Carlo spherical models). (g) Electrical conductivity of $PbSO_4$ with different grain sizes by calculation. (h) Statistical diagram of electrical conductivity of $PbSO_4$ nanoparticles. (i) Schematic diagram of tr-SPV measurements. (j) The tr-SPV measurements of perovskite films based on FTO, $PbSO_4$, and TiO_2.*

transport state,[33] which conformed to quadratic band crossings of surficial metallicity, realizing the unhindered electron transport across nanoparticle surface.[34,35] The metallicity on the surface of the $PbSO_4$ nanoparticle was further evaluated, with the results shown in Supporting Information Figures S11 and S12, $PbSO_4$ films with different grain sizes were prepared; also, Monte Carlo spherical models of $PbSO_4$ nanoparticles based on the normal distribution of the prepared nanoparticle sizes were created to calculate their electrical conductivities (Figure 3f and Supporting Information Figure S12). The calculated unit surface conductivity was similar under different particle size distributions (Figure 3g) and was comparable to the conductivity of common metals (~10^6 S m^{-1}). Experimentally, the conductivities of $PbSO_4$ films with different grain sizes also revealed similar conductivities (~1.1×10^{-4} S m^{-1}, Figure 3h and Supporting Information Figure S13a). This value was lower than the calculated value based on the ideal model but was undoubtedly higher than that of the bulk $PbSO_4$ material[36] (~1.0×10^{-6} S m^{-1}). This value was almost consistent with the values of commonly used TiO_2/SnO_2 ETMs.[37,38] The electron mobility experiment of $PbSO_4$ films was also performed and calculated (Supporting Information Figure S13b) to be 2.51×10^{-4} cm^2 V^{-1} s^{-1}, which was higher than TiO_2 (1.71×10^{-4} cm^2 V^{-1} s^{-1}).

Next, the electron extraction between the $PbSO_4$/perovskite interface was investigated by transient surface photovoltage (tr-SPV) measurements (Figure 3i).[39] Charge extraction in the range of 5 ns to 0.5 s was studied by noncontact SPV measurements excited by 5 ns above bandgap laser (1.8 eV). $PbSO_4$ showed a much faster rise and larger amplitude than FTO, meaning that $PbSO_4$ had

DOI: 10.31635/ccschem.024.202303502
Citation: *CCS Chem.* **2024**, 6, 2254–2263
Link to VoR: https://doi.org/10.31635/ccschem.024.202303502

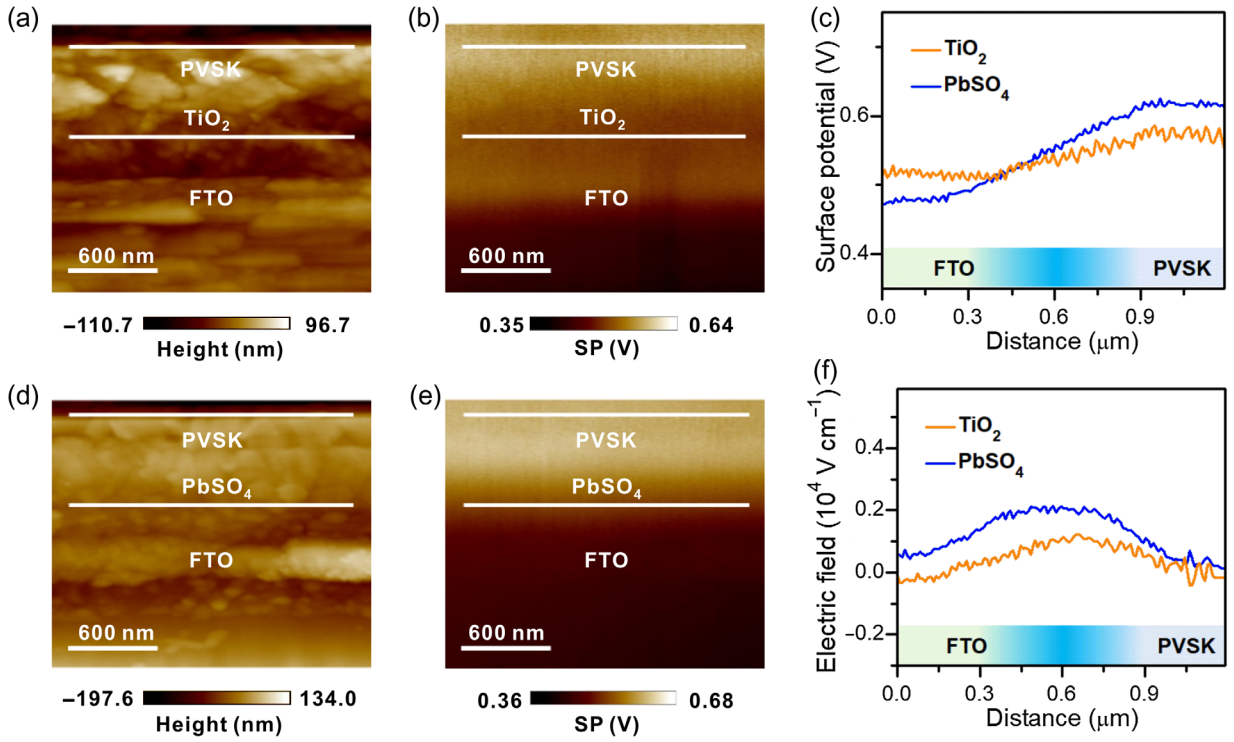

Figure 4 | *AFM topography images of devices with TiO_2 (a) and $PbSO_4$ (d). KPFM SP images were taken on the cross-sectional surface of devices with TiO_2 (b) and $PbSO_4$ (e). SP profile (c) and electric field distribution (f) of the cross-sectional surface of devices based on TiO_2 and $PbSO_4$.*

much better electron extraction properties than FTO (Figure 3j). The much faster tr-SPV signal (in the 5–20 ns) highlighted much better electron extraction capabilities of $PbSO_4$ compared with TiO_2. These analyses suggested that mainly charge transport channels existed in $PbSO_4$ nanoparticles with (011) surface and could be attributed to the nanoparticle surface with metal conductivity. The yielded metallicity on the (011) surface of the $PbSO_4$ nanoparticle promoted the transport of extracted electrons across the nanoparticle surface.

Additionally, KPFM characterizations of the perovskite cross-sections were carried out. The AFM topographic is shown in Figure 4a,d. The surface potential (SP) profile was extracted from Figure 4b,e. As shown in Figure 4c, the $PbSO_4$=based device revealed a significant potential drop at the FTO/perovskite interface compared with the control device. The local electric field distribution was obtained by taking the first derivative of SP profiles.[40] The stronger electric field was observed in the $PbSO_4$= based device (Figure 4f), indicating that introducing the $PbSO_4$ layer could effectively enhance the interfacial electron extraction and transport.[41,42] Similar conclusions were also drawn from PL spectra. The quenched fluorescence intensity was detected for the $PbSO_4$-based perovskite film, revealing enhanced electron extraction and transport (Supporting Information Figure S14). Further, Mott–Schottky measurements presented the $PbSO_4$-based device with a more significant slope than the control device, indicating that introducing $PbSO_4$ reduced the interface charge density (Supporting Information Figure S15). Space charge limited current (SCLC) tests were employed to evaluate perovskite films' electron trap-state densities.[43,44] The resulted showed a marked decreased from 4.4×10^{15} cm^{-3} to 2.7×10^{15} cm^{-3} for the control and $PbSO_4$-based device (Supporting Information Figure S16). Electrochemical impedance spectroscopy (EIS) tests revealed that the recombination resistance increased for the $PbSO_4$-based device compared with the control sample, suggesting that the $PbSO_4$ effectively inhibited charge recombination (Supporting Information Figure S17). The above results demonstrated that the $PbSO_4$ layer effectively promoted interfacial electron transport and suppressed the recombination.

Photovoltaic performance of devices

The PSCs with FTO/c-TiO_2 or $PbSO_4$/m-TiO_2/perovskite/Spiro-OMeTAD/Au structure were fabricated to evaluate the effect of $PbSO_4$ on cell performance (Supporting Information Figure S18). As shown in Figure 5a, the $PbSO_4$-based device exhibited negligible hysteresis behavior compared with the TiO_2-based device. The champion efficiency of the devices at optimal

DOI: 10.31635/ccschem.024.202303502
Citation: *CCS Chem.* **2024**, 6, 2254–2263
Link to VoR: https://doi.org/10.31635/ccschem.024.202303502

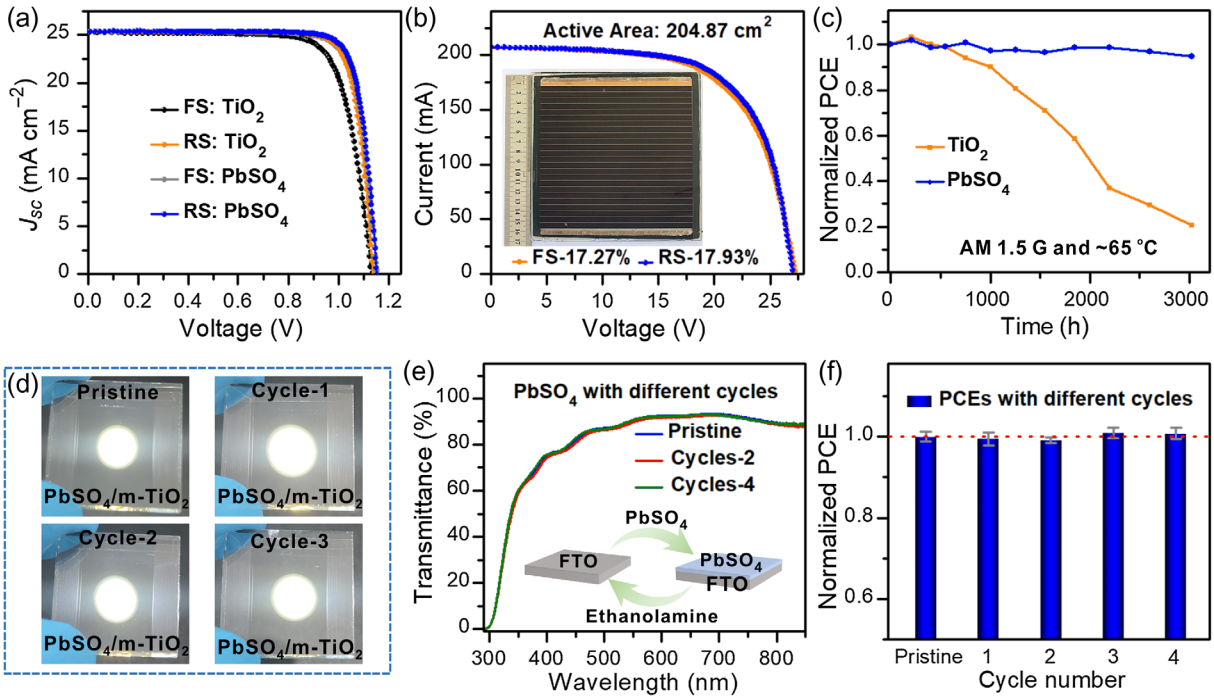

Figure 5 | *(a) Best J–V data of PSCs with TiO_2 and $PbSO_4$ obtained in forward (FS) and reverse (RS) scans. (b) I–V characteristics of the 204.87 cm^2 area PSC module. (c) Photostability at AM 1.5 G illumination and ~65 °C in N_2 atmosphere. (d) Photos of recycled substrates based on $PbSO_4$ at different cycles. (e) Transmission spectra of substrates based on $PbSO_4$ at different cycles. (f) Efficiencies of PSCs with $PbSO_4$ in different cycles.*

$PbSO_4$ thickness of ~20 nm, obtained by adjusting the concentration of $PbSO_4$ solution (Supporting Information Figure S19) was 24.1% for an active area of 0.1 cm^2, slightly higher than the values of PSCs with TiO_2 (23.7%, 0.1 cm^2) (Figure 5a, Supporting Information Figure S20 and Table S2). The average efficiency of devices with TiO_2 was 23.2 ± 0.5%, while the performance distribution for the $PbSO_4$-based PSCs with 23.7 ± 0.4% was observed (Supporting Information Figure S21). The champion efficiency of $PbSO_4$-based PSCs was further evaluated, which yielded a stabilized efficiency output of 23.6% (Supporting Information Figure S22). The large-area TiO_2- and $PbSO_4$-based PSCs with an area of 1.0 cm^2 were also prepared for performance evaluation (Supporting Information Figure S23 and Table S3). The best performances for PSCs based on TiO_2 and $PbSO_4$ were up to 21.9% and 22.3%, respectively, demonstrating a better performance of the $PbSO_4$-based PSC. The efficiency of the $PbSO_4$-based device was further certified as 21.7% with an area of 0.9974 cm^2 (Supporting Information Figure S24). The practical application of $PbSO_4$ was also evaluated for fabricating perovskite photovoltaic modules. As shown in Figure 5b, Supporting Information Figure S25, and Table S4, the efficiency reached 17.9% with an active area of 204.87 cm^2 and 16.8% with a designated area of 218.38 cm^2. A steady-state maximum power output of the module further verified the efficiency (Supporting Information Figure S25). Thus, the $PbSO_4$ film could realize interfacial electron extraction and transport from the perovskite layer more effectively to improve mainly the V_{oc} and cell performance.

Stabilities of devices

Since the stability of PSCs is an essential factor for commercialization, the PSCs with FTO/c-TiO_2 or $PbSO_4$/m-TiO_2/perovskite/phthalocyanine[45]/Au structure without encapsulation were fabricated to assess the effect of $PbSO_4$ on stability (Supporting Information Figure S26), due to the poor stability of Spiro-OMeTAD.[46] Photostability of the devices was performed at AM 1.5 G illumination and ~65 °C in N_2 atmosphere. The PSC with $PbSO_4$ remained at 90% of the original efficiency, whereas the device with TiO_2 retained 20% of the initial efficiency after 3000 h (Figure 5c). Thermal stability was performed at 85 °C with ~30% humidity in the air atmosphere. As shown in Supporting Information Figure S27a, the device with $PbSO_4$ retained more than 90% of the initial efficiency after 3000 h, while the TiO_2-based device almost failed during this period. We further tested the moisture stability with a humidity of ~65% in the air. The device with $PbSO_4$ retained 90% of the original efficiency after 5000 h, while the control PSC almost failed under the same conditions (Supporting Information Figure S27b). The above results revealed

DOI: 10.31635/ccschem.024.202303502
Citation: *CCS Chem.* **2024**, 6, 2254–2263
Link to VoR: https://doi.org/10.31635/ccschem.024.202303502

that $PbSO_4$ as a stable ETM assisted the preparation of high-quality perovskite film with reduced defects, and promoted interfacial electron extraction and transport, thereby effectively improving the cell stabilities.

Recyclability of conductive substrate

Recycling valuable materials from PSCs is urgent and necessary for commercialization and environmental demands.[47,48] The $PbSO_4$ can be well dissolved in ethanolamine solution; thus, used as the solvent for the $PbSO_4$ device fabrication process. A simple ethanolamine solution washing efficiently recovered the FTO substrate with $PbSO_4$. To evaluate this conjecture, the $PbSO_4$- and m-TiO_2-based substrates were washed with ethanolamine solution. This cycling process was conducted several times. As shown in Figure 5d and Supporting Information Figure S28, the $PbSO_4$ and m-TiO_2 layer could be well-removed by dissolving the $PbSO_4$ layer with ethanolamine washing. The recovered FTO substrates maintained the original transmittance value (Figure 5e). The corresponding PSCs were also fabricated with recycled substrates. As expected, compared with the device with a new FTO substrate, the PSCs with recovered FTO substrates based on $PbSO_4$ displayed similar cell performances (Figure 5f). These results demonstrate that the FTO substrate coated with $PbSO_4$ could be well-recovered by simple ethanolamine washing.

Conclusion

We developed $PbSO_4$ wide-bandgap nanoparticles with a conductive (011) surface as a novel ETM, which revealed access to the recycling of PSCs, including recycling of valuable conductive substrates. The introduced $PbSO_4$ film promoted interfacial electron extraction and transport and reduced charge recombination. The $PbSO_4$-based PSCs exhibited an exceptional cell PCE of 24.1% and remarkably improved stability compared with the device with TiO_2. The certified efficiency of 17.9% for an active area of 204.9 cm^2 submodule with $PbSO_4$ was realized. Most importantly, the $PbSO_4$ film could be easily removed from the conductive substrate by a simple solution washing process to realize recovery of the conductive substrate and decrease the cost of constructing PSCs. This work provides a sustainable strategy to design a new-type ETM with a metallicity surface, fabricating low-cost, efficient, and recyclable PSCs, thereby accelerating the commercialization of PSCs.

Supporting Information

Supporting Information is available and includes detailed methods of solar cell fabrication, computational methods, and device characterization, viz, XRD, SEM images, AFM images, UV–vis and PL spectra, certified efficiencies reports, and photovoltaic performances of the devices.

Conflict of Interest

The authors declare no competing interests.

Acknowledgments

We acknowledge the National Natural Science Foundation of China (grant nos. 22075116, 22371096, and 22221001), Fundamental Research Funds for the Central Universities of China (grant no. lzujbky-2021-ey10), the U.S. Department of Energy (grant no. DE-FG02-07ER46427), and European Union's Framework Programme for Research and Innovation HORIZON EUROPE (2021–2027) under the Marie Skłodowska-Curie Action Postdoctoral Fellowships (European Fellowship; grant no. 101061809 HyPerGreen). We gratefully acknowledge Dr. Thomas Dittrich for providing the HZB SPV lab facilities.

References

1. Li, C.; Wang, X.; Bi, E.; Jiang, F.; Park, S. M.; Li, Y.; Chen, L.; Wang, Z.; Zeng, L.; Chen, H.; Liu, Y.; Grice, C. R.; Abudulimu, A.; Chung, J.; Xian, Y.; Zhu, T.; Lai, H.; Chen, B.; Ellingson, R. J.; Fu, F.; Ginger, D. S.; Song, Z.; Sargent, E. H.; Yan, Y. Rational Design of Lewis Base Molecules for Stable and Efficient Inverted Perovskite Solar Cells. *Science* **2023**, *379*, 690–694.
2. Sheng, W.; Yang, J.; Li, X.; Zhang, J.; Su, Y.; Zhong, Y.; Zhang, Y.; Gong, L.; Tan, L.; Chen, Y. Dual Triplet Sensitization Strategy for Efficient and Stable Triplet–Triplet Annihilation Upconversion Perovskite Solar Cells. *CCS Chem.* **2023**, *5*, 729–740.
3. Chen, S.; Deng, Y.; Xiao, X.; Xu, S.; Rudd, P. N.; Huang, J. Preventing Lead Leakage with Built-in Resin Layers for Sustainable Perovskite Solar Cells. *Nat. Sustain.* **2021**, *4*, 636–643.
4. Ye, Y.; Yin, Y.; Chen, Y.; Li, S.; Li, L.; Yamauchi, Y. Metal-Organic Framework Materials in Perovskite Solar Cells: Recent Advancements and Perspectives. *Small* **2023**, *19*, 2208119.
5. Xiao, G.-B.; Wang, L.-Y.; Mu, X.-J.; Zou, X.-X.; Wu, Y.-Y.; Cao, J. Lead and Iodide Fixation by Thiol Copper Porphyrin for Stable and Environmental-Friendly Perovskite Solar Cells. *CCS Chem.* **2021**, *3*, 25–36.
6. Yin, Y.; Wang, M.; Malgras, V.; Yamauchi, Y. Stable and Efficient Tin-Based Perovskite Solar Cell via Semiconducting–Insulating Structure. *ACS Appl. Energy Mater.* **2020**, *3*, 10447–10452.
7. Zhang, T.; Wang, F.; Kim, H.-B.; Choi, I.-W.; Wang, C.; Cho, E.; Konefal, R.; Puttisong, Y.; Terado, K.; Kobera, L.; Chen, M.; Yang, M.; Bai, S.; Yang, B.; Suo, J.; Yang, S.-C.; Liu, X.; Fu, F.; Yoshida, H.; Chen, W. M.; Brus, J.; Coropceanu, V.; Hagfeldt, A.; Brédas, J.-L.; Fahlman, M.; Kim, D. S.; Hu, Z.; Gao, F. Ion-Modulated Radical Doping of Spiro-OMeTAD for More

DOI: 10.31635/ccschem.024.202303502
Citation: *CCS Chem.* **2024**, 6, 2254–2263
Link to VoR: https://doi.org/10.31635/ccschem.024.202303502

Efficient and Stable Perovskite Solar Cells. *Science* **2022**, *377*, 495–501.
8. Park, J.; Kim, J.; Yun, H. S.; Paik, M. J.; Noh, E.; Mun, H. J.; Kim, M. G.; Shin, T. J.; Seok, S. I. Controlled Growth of Perovskite Layers with Volatile Alkylammonium Chlorides. *Nature* **2023**, *616*, 724–730.
9. Zhao, Y.; Ma, F.; Qu, Z.; Yu, S.; Shen, T.; Deng, H.-X.; Chu, X.; Peng, X.; Yuan, Y.; Zhang, X.; You, J. Inactive $(PbI_2)_2RbCl$ Stabilizes Perovskite Films for Efficient Solar Cells. *Science* **2022**, *377*, 531–534.
10. Yun, H.-S.; Kwon, H. W.; Paik, M. J.; Hong, S.; Kim, J.; Noh, E.; Park, J.; Lee, Y.; Il Seok, S. Ethanol-Based Green-Solution Processing of α-Formamidinium Lead Triiodide Perovskite Layers. *Nat. Energy* **2022**, *7*, 828–834.
11. Altinkaya, C.; Aydin, E.; Ugur, E.; Isikgor, F. H.; Subbiah, A. S.; De Bastiani, M.; Liu, J.; Babayigit, A.; Allen, T. G.; Laquai, F.; Yildiz, A.; De Wolf, S. Tin Oxide Electron-Selective Layers for Efficient, Stable, and Scalable Perovskite Solar Cells. *Adv. Mater.* **2021**, *33*, 2005504.
12. Park, S. Y.; Zhu, K. Advances in SnO_2 for Efficient and Stable n-i-p Perovskite Solar Cells. *Adv. Mater.* **2022**, *34*, 2110438.
13. Ding, Y.; Ding, B.; Kanda, H.; Usiobo, O. J.; Gallet, T.; Yang, Z.; Liu, Y.; Huang, H.; Sheng, J.; Liu, C.; Yang, Y.; Queloz, V. I. E.; Zhang, X.; Audinot, J. N.; Redinger, A.; Dang, W.; Mosconic, E.; Luo, W.; De Angelis, F.; Wang, M.; Dorflinger, P.; Armer, M.; Schmid, V.; Wang, R.; Brooks, K. G.; Wu, J.; Dyakonov, V.; Yang, G.; Dai, S.; Dyson, P. J.; Nazeeruddin, M. K. Single-Crystalline TiO_2 Nanoparticles for Stable and Efficient Perovskite Modules. *Nat. Nanotechnol.* **2022**, *17*, 598–605.
14. Wu, P.; Wang, S.; Li, X.; Zhang, F. Advances in SnO_2-Based Perovskite Solar Cells: From Preparation to Photovoltaic Applications. *J. Mater. Chem. A* **2021**, *9*, 19554–19588.
15. Tan, C.; Xu, W.; Huan, Y.; Wu, B.; Qin, T.; Gao, D. Increasing Stability of SnO_2-Based Perovskite Solar Cells by Introducing an Anionic Conjugated Polyelectrolyte for Interfacial Adjustment. *ACS Appl. Mater. Interfaces* **2021**, *13*, 24575–24581.
16. Zhuang, Q.; Zhang, C.; Gong, C.; Li, H.; Li, H.; Zhang, Z.; Yang, H.; Chen, J.; Zang, Z. Tailoring Multifunctional Anion Modifiers to Modulate Interfacial Chemical Interactions for Efficient and Stable Perovskite Solar Cells. *Nano Energy* **2022**, *102*, 107747.
17. Jeong, J.; Kim, M.; Seo, J.; Lu, H.; Ahlawat, P.; Mishra, A.; Yang, Y.; Hope, M. A.; Eickemeyer, F. T.; Kim, M.; Yoon, Y. J.; Choi, I. W.; Darwich, B. P.; Choi, S. J.; Jo, Y.; Lee, J. H.; Walker, B.; Zakeeruddin, S. M.; Emsley, L.; Rothlisberger, U.; Hagfeldt, A.; Kim, D. S.; Grätzel, M.; Kim, J. Y. Pseudo-Halide Anion Engineering for α-$FAPbI_3$ Perovskite Solar Cells. *Nature* **2021**, *592*, 381–385.
18. Cheng, Y.; Wu, H.; Ma, J.; Li, P.; Gu, Z.; Zang, S.; Han, L.; Zhang, Y.; Song, Y. Droplet Manipulation and Crystallization Regulation in Inkjet-Printed Perovskite Film Formation. *CCS Chem.* **2022**, *4*, 1465–1485.
19. Luo, X.; Shen, Z.; Shen, Y.; Su, Z.; Gao, X.; Wang, Y.; Han, Q.; Han, L. Effective Passivation with Self-Organized Molecules for Perovskite Photovoltaics. *Adv. Mater.* **2022**, *34*, 2202100.
20. Shen, Z.; Han, Q.; Luo, X.; Shen, Y.; Wang, T.; Zhang, C.; Wang, Y.; Chen, H.; Yang, X.; Zhang, Y.; Han, L. Crystal-Array-Assisted Growth of Perovskite Absorption Layer for Efficient and Stable Solar Cell. *Energy Environ. Sci.* **2022**, *15*, 1078–1085.
21. Xiao, G.-B.; Yu, Z.-F.; Cao, J.; Tang, Y. Encapsulation and Regeneration of Perovskite Film by in Situ Forming Cobalt Porphyrin Polymer for Efficient Photovoltaics. *CCS Chem.* **2020**, *2*, 488–494.
22. Wang, C.; Gao, Y.; Qiu, Z.-L.; Sun, P.-P.; Shibayama, N.; Zhang, Z.; Xiong, Q.; Ren, F.; Lien, S.-Y.; Liang, L.; Zhang, J.; Tan, Y.-Z.; Gao, P. D^{6h} Symmetric Radical Donor–Acceptor Nanographene Modulated Interfacial Carrier Transfer for High-Performance Perovskite Solar Cells. *CCS Chem.* **2022**, *5*, 2159–2170.
23. Yoo, J. J.; Seo, G.; Chua, M. R.; Park, T. G.; Lu, Y.; Rotermund, F.; Kim, Y.-K.; Moon, C. S.; Jeon, N. J.; Correa-Baena, J.-P.; Bulović, V.; Shin, S. S.; Bawendi, M. G.; Seo, J. Efficient Perovskite Solar Cells via Improved Carrier Management. *Nature* **2021**, *590*, 587–593.
24. Kim, M.; Jeong, J.; Lu, H.; Lee, T. K.; Eickemeyer, F. T.; Liu, Y.; Choi, I. W.; Choi, S. J.; Jo, Y.; Kim, H.-B.; Mo, S.-I.; Kim, Y.-K.; Lee, H.; An, N. G.; Cho, S.; Tress, W. R.; Zakeeruddin, S. M.; Hagfeldt, A.; Kim, J. Y.; Grätzel, M.; Kim, D. S. Conformal Quantum Dot-SnO_2 Layers as Electron Transporters for Efficient Perovskite Solar Cells. *Science* **2022**, *375*, 302–306.
25. Min, H.; Lee, D. Y.; Kim, J.; Kim, G.; Lee, K. S.; Kim, J.; Paik, M. J.; Kim, Y. K.; Kim, K. S.; Kim, M. G.; Shin, T. J.; Il Seok, S. Perovskite Solar Cells with Atomically Coherent Interlayers on SnO_2 Electrodes. *Nature* **2021**, *598*, 444–450.
26. Song, Z.; McElvany, C. L.; Phillips, A. B.; Celik, I.; Krantz, P. W.; Watthage, S. C.; Liyanage, G. K.; Apul, D.; Heben, M. J. A Technoeconomic Analysis of Perovskite Solar Module Manufacturing with Low-Cost Materials and Techniques. *Energy Environ. Sci.* **2017**, *10*, 1297–1305.
27. Cai, M.; Wu, Y.; Chen, H.; Yang, X.; Qiang, Y.; Han, L. Cost-Performance Analysis of Perovskite Solar Modules. *Adv. Sci.* **2017**, *4*, 1600269.
28. Yang, S.; Chen, S.; Mosconi, E.; Fang, Y.; Xiao, X.; Wang, C.; Zhou, Y.; Yu, Z.; Zhao, J.; Gao, Y.; De Angelis, F.; Huang, J. Stabilizing Halide Perovskite Surfaces for Solar Cell Operation with Wide-Bandgap Lead Oxysalts. *Science* **2019**, *365*, 473–478.
29. Zhang, H.; Liu, C.-X.; Qi, X.-L.; Dai, X.; Fang, Z.; Zhang, S.-C. Topological Insulators in Bi_2Se_3, Bi_2Te_3, and Sb_2Te_3 with a Single Dirac Cone on the Surface. *Nat. Phys.* **2009**, *5*, 438–442.
30. Chen, Y. L.; Analytis, J. G.; Chu, J. H.; Liu, Z. K.; Mo, S. K.; Qi, X. L.; Zhang, H. J.; Lu, D. H.; Dai, X.; Fang, Z.; Zhang, S. C.; Fisher, I. R.; Hussain, Z.; Shen, Z. X. Experimental Realization of a Three-Dimensional Topological Insulator, Bi_2Te_3. *Science* **2009**, *325*, 178–181.
31. Foa Torres, L. E. F.; Perez-Piskunow, P. M.; Balseiro, C. A.; Usaj, G. Multiterminal Conductance of a Floquet Topological Insulator. *Phys. Rev. Lett.* **2014**, *113*, 266801.

DOI: 10.31635/ccschem.024.202303502
Citation: *CCS Chem.* **2024**, 6, 2254–2263
Link to VoR: https://doi.org/10.31635/ccschem.024.202303502

32. Li, Z.; Zhao, Y.; Wang, X.; Sun, Y.; Zhao, Z.; Li, Y.; Zhou, H.; Chen, Q. Cost Analysis of Perovskite Tandem Photovoltaics. *Joule* **2018**, *2*, 1559–1572.
33. Sun, Y.; Wu, S.-C.; Yan, B. Topological Surface States and Fermi Arcs of the Noncentrosymmetric Weyl Semimetals TaAs, TaP, NbAs, and NbP. *Phys. Rev. B* **2015**, *92*, 115428.
34. Qi, X.-L.; Zhang, S.-C. Topological Insulators and Superconductors. *Rev. Mod. Phys.* **2011**, *83*, 1057–1110.
35. Lv, B. Q.; Qian, T.; Ding, H. Experimental Perspective on Three-Dimensional Topological Semimetals. *Rev. Mod. Phys.* **2021**, *93*, 025002.
36. Garche, J.; Dyer, C.; Moseley, P. T.; Ogumi, Z.; Rand, D. A.; Scrosati, B., *Encyclopedia of Electrochemical Power Sources*; Newnes: Amsterdam, The Netherlands, **2013**.
37. Li, Z.; Wang, C.; Sun, P.-P.; Zhang, Z.; Zhou, Q.; Du, Y.; Xu, J.; Chen, Y.; Xiong, Q.; Ding, L.; Nazeeruddin, M. K.; Gao, P. In-Situ Peptization of WO_3 in Alkaline SnO_2 Colloid for Stable Perovskite Solar Cells with Record Fill-Factor Approaching the Shockley–Queisser Limit. *Nano Energy* **2022**, *100*, 107468.
38. Shi, X.; Ding, Y.; Zhou, S.; Zhang, B.; Cai, M.; Yao, J.; Hu, L.; Wu, J.; Dai, S.; Nazeeruddin, M. K. Enhanced Interfacial Binding and Electron Extraction Using Boron-Doped TiO_2 for Highly Efficient Hysteresis-Free Perovskite Solar Cells. *Adv. Sci.* **2019**, *6*, 1901213.
39. Levine, I.; Al-Ashouri, A.; Musiienko, A.; Hempel, H.; Magomedov, A.; Drevilkauskaite, A.; Getautis, V.; Menzel, D.; Hinrichs, K.; Unold, T.; Albrecht, S.; Dittrich, T. Charge Transfer Rates and Electron Trapping at Buried Interfaces of Perovskite Solar Cells. *Joule* **2021**, *5*, 2915–2933.
40. Bergmann, V. W.; Weber, S. A.; Javier Ramos, F.; Nazeeruddin, M. K.; Grätzel, M.; Li, D.; Domanski, A. L.; Lieberwirth, I.; Ahmad, S.; Berger, R. Real-Space Observation of Unbalanced Charge Distribution Inside a Perovskite-Sensitized Solar Cell. *Nat. Commun.* **2014**, *5*, 5001.
41. Zhang, M.; Chen, Q.; Xue, R.; Zhan, Y.; Wang, C.; Lai, J.; Yang, J.; Lin, H.; Yao, J.; Li, Y.; Chen, L.; Li, Y. Reconfiguration of Interfacial Energy Band Structure for High-Performance Inverted Structure Perovskite Solar Cells. *Nat. Commun.* **2019**, *10*, 4593.
42. Jiang, X.; Wang, F.; Wei, Q.; Li, H.; Shang, Y.; Zhou, W.; Wang, C.; Cheng, P.; Chen, Q.; Chen, L.; Ning, Z. Ultra-High Open-Circuit Voltage of Tin Perovskite Solar Cells via an Electron Transporting Layer Design. *Nat. Commun.* **2020**, *11*, 1245.
43. Dou, J.; Zhu, C.; Wang, H.; Han, Y.; Ma, S.; Niu, X.; Li, N.; Shi, C.; Qiu, Z.; Zhou, H.; Bai, Y.; Chen, Q. Synergistic Effects of Eu-MOF on Perovskite Solar Cells with Improved Stability. *Adv. Mater.* **2021**, *33*, e2102947.
44. Zhao, J. H.; Mu, X.; Wang, L.; Fang, Z.; Zou, X.; Cao, J. Homogeneously Large Polarons in Aromatic Passivators Improves Charge Transport Between Perovskite Grains for >24% Efficiency in Photovoltaics. *Angew. Chem. Int. Ed.* **2022**, *61*, e202116308.
45. Yu, Z.; Wang, L.; Mu, X.; Chen, C.-C.; Wu, Y.; Cao, J.; Tang, Y. Intramolecular Electric Field Construction in Metal Phthalocyanine as Dopant-Free Hole Transporting Material for Stable Perovskite Solar Cells with >21% Efficiency. *Angew. Chem. Int. Ed.* **2021**, *60*, 6294–6299.
46. Yao, Z.; Zhang, F.; Guo, Y.; Wu, H.; He, L.; Liu, Z.; Cai, B.; Guo, Y.; Brett, C. J.; Li, Y.; Srambickal, C. V.; Yang, X.; Chen, G.; Widengren, J.; Liu, D.; Gardner, J. M.; Kloo, L.; Sun, L. Conformational and Compositional Tuning of Phenanthrocarbazole-Based Dopant-Free Hole-Transport Polymers Boosting the Performance of Perovskite Solar Cells. *J. Am. Chem. Soc.* **2020**, *142*, 17681–17692.
47. Chen, B.; Fei, C.; Chen, S.; Gu, H.; Xiao, X.; Huang, J. Recycling Lead and Transparent Conductors from Perovskite Solar Modules. *Nat. Commun.* **2021**, *12*, 5859–5868.
48. Liu, F.-W.; Biesold, G.; Zhang, M.; Lawless, R.; Correa-Baena, J.-P.; Chueh, Y.-L.; Lin, Z. Recycling and Recovery of Perovskite Solar Cells. *Mater. Today* **2021**, *43*, 185–197.

DOI: 10.31635/ccschem.024.202303502
Citation: *CCS Chem.* **2024**, 6, 2254–2263
Link to VoR: https://doi.org/10.31635/ccschem.024.202303502